2025 IEEE/SICE International Symposium on System Integration (SII)
January 21-24, 2025, Munich, Germany

Development of a Soft Growing Actuator for Automated Cystoscope Insertion

K. Kishino, R. Okuma, F. Ito, *Member, IEEE,* H. Yamanaka, M. Komeya, and T. Nakamura, *Member, IEEE*

Abstract— **This study presents the first prototype of an insertion mechanism designed to reduce pain during cystoscope insertion. Traditional cystoscopy often causes discomfort as the cystoscope rubs against the urethral wall and its tip impacts the curved urethra. To address this issue, this study focuses on developing a "painless" automatic insertion mechanism for cystoscopy in the urethra, prostate, and bladder using a soft growing actuator. The paper introduces a compact soft growing actuator made from a low-friction material capable of inverted growth. The prototype actuator extended to a maximum length of 140 mm in just 0.10 seconds, with no significant variation in the elongation-time relationship when air pressure was applied at 70–90 kPa. The prototype successfully guided a cystoscope-like wire from the urethral entrance to the bladder within an S-tube that replicates the scale and curvature of the human urethra. These findings suggest that the proposed cystoscope insertion mechanism, utilizing a soft growing actuator, has the potential to enable automated cystoscopy for rapid and painless examination of the human urethra.**

I. Introduction

Bladder cancer is a malignant tumor that develops from the urothelial mucosa of the bladder, with nearly all cases being urothelial carcinomas originating from urothelial cells [1]. It is the ninth most common cancer worldwide and the 13th leading cause of cancer-related death [2]. The incidence rate increases for both men and women starting in their 60s and is about four times higher in men than in women. Additionally, bladder cancer has a high recurrence rate, with up to 50% of cases recurring within 5 years and 20% showing progression [3]. Consequently, periodic cystoscopy of the bladder is recommended for early detection of recurrence and progression.

Cystoscopy is crucial for the diagnosis, treatment, and follow-up of bladder cancer. Currently, flexible cystoscopes are employed for these procedures [4]. The cystoscope is inserted through the urethra while physiological saline solution is injected, allowing it to be advanced through the urethra to reach the prostate and bladder. This technique enables direct visualization of the urethra, prostate, and bladder, facilitating the identification of bladder cancer, bladder stones, bladder foreign bodies and other urological lesions. However, pain during the procedure is a notable concern when using a flexible cystoscope. This pain is primarily caused by damage to the urethral inner wall due to the cystoscope rubbing against it or the camera tip striking the curved urethra. The male urethra, in particular, is long, narrow, and has a three-dimensional curvature, leading to significant pain, especially at the prepubic and sub-pubic bends [5]. Methods such as applying gel to the endoscope and administering anesthesia have been employed to address pain during cystoscopy. However, these approaches do not effectively reduce the fundamental invasiveness of the procedure. Minimizing this invasiveness requires a skilled physician to carefully manipulate the cystoscope during insertion. Thus, there is a need for an automated cystoscope insertion method that reduces pain. We believe that such a method would alleviate the burden on both physicians and patients during examinations and increase the frequency of screening opportunities.

Previous studies have introduced various insertion mechanisms in endoscopes used for intravital examinations to reduce invasiveness. These mechanisms include capsule endoscopes [6-7] and double-balloon endoscopes [8-9]. Capsule endoscopes are wireless and coated with minimally invasive material, allowing for painless examinations. However, because they are operated remotely, controlling their direction and speed is challenging, and there is a risk of the capsule remaining inside the body. The double-balloon endoscope features a pneumatically driven dual-balloon design that allows for minimally invasive insertion and precise directional control at bends. Despite these advantages, its insertion technique is complex, requiring two personnel and a significant amount of time. Therefore, there is a need for a new insertion mechanism that facilitates low-friction, smooth examinations in narrow spaces (with a minimum diameter of 6 mm) such as the urethra, prostate, and bladder.

The purpose of this study was to develop a "painless" automatic insertion mechanism using a soft growing actuator for cystoscopy in narrow spaces, such as the urethra, prostate, and bladder. The soft growing actuator was constructed from a thin-walled tube, with one end attached to a pressurizer and the other end sealed and folded inward to prevent air leakage. When air pressure was applied through the pressurizer, the inwardly folded tube was pushed by the air pressure, causing it to flip outward and extend [10]. This extension method prevents friction, as the tube unfolds without sliding against the surrounding environment [11]. The mechanism operates solely by pressurizing and depressurizing air, making it simpler to use than a double-balloon endoscope with a similar pneumatic drive. As the pneumatic tube inverts and extends, the cystoscope mounted inside the soft growing actuator is

K. Kishino, R. Okuma, F. Ito and T. Nakamura are with the Department of Precision Mechanics, Faculty of Science and Engineering, Chuo University, 1-13-27 Kasuga, Bunkyo-Ku, Tokyo, 112-8551, Japan (corresponding author to provide e-mail: k_kishino@bio.mech.chuo-u.ac.jp).

H. Yamanaka and M. Komeya are with the Department of Urology, Faculty of Medicine, Yokohama City University, 3-9 Hukuura, Kanazawa-Ku, Yokohama 236-0004, Japan (e-mail: komeyam@yokohama-cu.ac.jp).

guided through the urethra, avoiding contact with the urethral wall or collisions with the curved canal.

Conventional soft growing actuators have been developed to mimic plant growth behavior and enable movement into challenging and delicate environments, such as disaster sites [10-13]. However, the prototype soft growing actuators used in these studies typically had inner diameters of about 25 mm. While a smaller soft growing actuator with an inner diameter of approximately 1.8 mm has also been developed [10], its driving performance has not yet been reported. Reducing the size of the actuator results in a smaller pressure-sensitive area at the inverted tip, but the endoscope's thickness remains unchanged. Consequently, the endoscope's diameter increases relative to the inner diameter of the tube, reducing the force that can be applied. Therefore, designing a compact soft growing actuator with an integrated endoscope necessitates careful consideration of the film's pressure resistance and the force it can exert.

This study proposes a compact, invertible soft growing actuator made of low-friction material to develop a “painless” automatic insertion mechanism. The aim of this study was to establish a method for developing a soft growing actuator that can invert and extend even at a small size, demonstrating that such an actuator can navigate through an S-shaped tube resembling a urethra. To achieve this, we detail the fabrication method of the actuator based on a pressure-resistant model and present the results of an experiment in which the soft growing actuator successfully passed through an S-shaped space that mimicked the urethra.

Chapter 2 outlines the automatic insertion mechanism and the pressure-resistant model, while Chapter 3 details the fabrication method of the soft growing actuator based on this model. Chapter 4 discusses the basic characteristics of the fabricated soft growing actuator, and Chapter 5 covers the S-tube experiment. Finally, Chapter 6 presents the concluding remarks and future perspectives.

II. Design

This study proposes a soft growing actuator for use in the automatic insertion mechanism of a cystoscope. This chapter provides an overview of the automatic insertion mechanism, the driving principle of the soft growing actuator, and the pressure-resistant model.

A. Mechanism Overview

Fig. 1 provides an overview of the proposed automatic cystoscope insertion mechanism, which comprises a compressor, air regulator, pressurizing chamber, soft growing actuator, and cystoscope. Air is supplied to the soft growing actuator from the compressor through an air regulator and pressurization chamber. When air pressure extends the actuator, the cystoscope attached to the soft growing actuator is inserted into the urethra. This paper focuses on developing a soft growing actuator and its insertion mechanism without utilizing a pressurization chamber.

B. Soft Growing Actuator Driving Principle

Figure 2 illustrates the extension process of the soft growing actuator, which is driven by the motions shown in Fig. 2(a), 2(b), and 2(c). (a) One end of the soft growing actuator is welded closed to prevent air leakage and then folded back inside the actuator. The length of this folded portion represents the maximum length that can be inverted or extended. The other end is taped to an air tube to prevent air leakage. (b) Air pressure is applied through the air tube inside the soft growing actuator, exerting force on a flap at the actuator’s tip. (c) The pneumatic pressure pushes the flap outward, causing the inner tube to flip outward. This mechanism allows the actuator body to extend without sliding against the surrounding environment. The soft growing actuator operates by sequentially performing these steps (a) to (c).

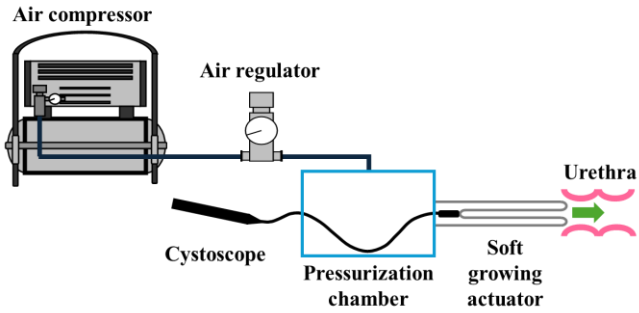

Figure 1. Equipment overview. Air is supplied to the soft growing actuator from a compressor through an air regulator and a pressurization chamber. A cystoscope is attached to the soft growing actuator, and the cystoscope is inserted into the urethra when the soft growing actuator is extended by air pressure.

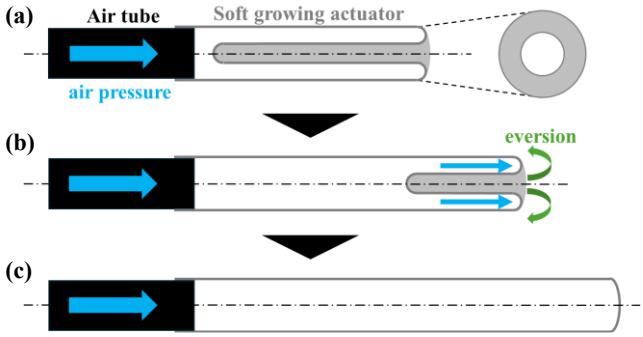

Figure 2. Operating principle of soft growing actuator. Cross-sectional view of the thin-walled tubular soft growing actuator connected to the pneumatic tube.

TABLE I Parameter for Modeling Soft Growing Actuator

Symbols	*Description*	*Unit*
r	Radius of cystoscope	[mm]
R	Inner radius of cylinder	[mm]
t	Thickness of cylinder	[mm]
B	Width of cylinder	[mm]
E	Modulus of elasticity	[MPa]
p	Internal pressure	[kPa]
F	Force applied to retract the endoscope	[N]
F_t	Circumferential force on cylinder	[N]

C. *Soft Growing Actuator Requirements*

The requirements for the soft growing actuator to be developed are as follows.

- Invertible material
- Smooth extension with minimal friction against the surrounding and internal cystoscope
- No air leaks
- An outer diameter of approximately 6 mm and an extensible length of approximately 200–230 mm to accommodate the male urethra (diameter 6–15 mm, length 180–200 mm).
- The following pressure-resistant model conditions are satisfied.

D. *Retractive Force Model for Soft Growing Actuator*

Fig. 3(a) illustrates the mechanical equilibrium state in the axial direction when air pressure is applied inside the soft growing actuator. Table 1 provides the parameters relevant to this figure. Based on the balance of axial forces, the retraction force F exerted on the cystoscope by the soft growing actuator can be expressed using Equation (1).

$$F = \pi p\{(R + \Delta R)^2 - (r + t)^2\} \tag{1}$$

E. *Pressure-resistant Model of Soft Growing Actuator*

Fig. 3(b) shows the mechanical equilibrium state in the radial direction when air pressure is applied inside the soft growing actuator. Table 1 lists the parameters related to this figure. From the balance of forces in the radial direction, the change in radius, ΔR, can be expressed using Equation (2).

$$\Delta R = \frac{R^2}{tE} p \tag{2}$$

By substituting Equation (2) into Equation (1), we obtain Equation (3).

$$F = \pi p \left\{ \left(R + \frac{R^2}{tE} p \right)^2 - (r + t)^2 \right\} \tag{3}$$

Therefore, the relationship between the elastic modulus and pressure is given by Equation (4).

$$E = \frac{p}{\left(\sqrt{\frac{F}{\pi p} + (r + t)^2} - R \right) \frac{t}{R^2}} \tag{4}$$

The numerical value of each parameter is determined. From the [10], the wall thickness t of the soft growing actuator is assumed to be between 0.05 and 0.08 mm, with $t \leq 0.08$ mm. Given that the cystoscope has a thickness of 3 mm, its radius r was set to 1.5 mm. Considering the urethral diameter, the initial inner diameter R of the soft growing actuator was set to 3 mm. The force required to manually insert the cystoscope into the rubber tube was measured five times using a digital force gauge, yielding an average result of approximately 4 N. Consequently, the retraction force F for the cystoscope was set to 4 N. Substituting these parameter values into Equation (4) produced a graph showing the relationship between the elastic modulus and pressure, as illustrated in Fig. 4. As $t \leq 0.08$ mm, the elastic modulus of the material used must be above this line for each pressure. Based on this model, a soft growing actuator was developed.

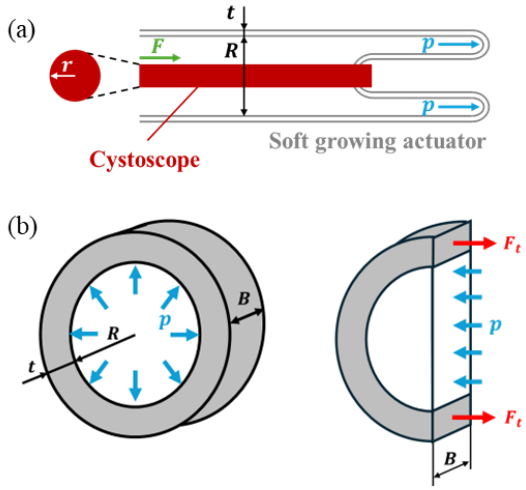

Figure 3. Mechanical equilibrium when air pressure is applied inside the soft growing actuator. (a) Axial direction. (b) Radial direction.

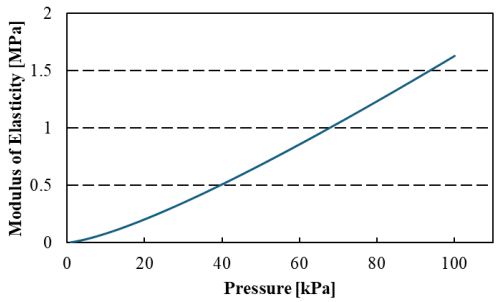

Figure 4. The relationship between modulus of elasticity and pressure in soft growing actuator.

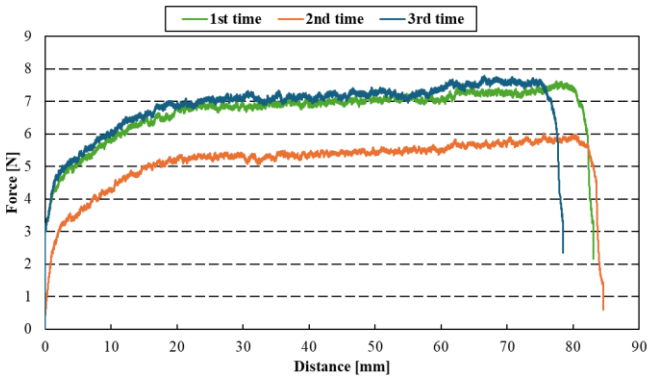

Figure 5. Load-displacement curves of polyethylene selected as material for soft growing actuator.

III. DEVELOPMENT

This chapter describes the methodology for developing a soft growing actuator based on the requirements and a pressure-resistant model.

A. Material Selection

When selecting the material for the soft growing actuator, it must meet the following conditions: (a) comply with the pressure resistance model, (b) possess flexibility and low friction to facilitate counter-rotational extension, and (c) have a heat resistance temperature suitable for sealing with a sealer. Considering these requirements, polyethylene (Maruman, polyethylene bag with zipper, 0.06 mm thick) was chosen as the material.

During the material selection process, a tensile tester (AIKOH ENGINEERING, MODEL-1308U) was used to assess the tensile properties of the polyethylene (PE) sheets. The test specimens adhered to the standard JIS K-6251-8. The load-displacement curves obtained from the tensile test are presented in Fig. 5. The relationship between the internal pressure p and the force F_t acting in the circumferential direction of the tube is described by Equation (5), based on the force balance in the cross-section of the tube as shown in Fig. 3(b).

$$p = \frac{F_t}{RB} \tag{5}$$

The load in the load–displacement curve corresponds to F_t. Based on the results of the tensile tests, F_t should be less than 2 N, assuming that the material is used in the elastic deformation zone. With a tube width B = 4 mm, the internal pressure (p) must be less than 166 kPa. The PE sheet used is low-density polyethylene (LDPE) with a modulus of approximately 150 MPa. The modulus of elasticity for the LDPE sheet exceeds the broken line for $p \leq 166$ kPa in the modulus-pressure relationship shown in Fig. 4. Thus, the PE sheet meets the requirements of the pressure-resistant model.

B. Fabrication Method

The soft growing actuator was fabricated using the following method: The fabrication process of the inverted elongated tube is illustrated in Fig. 6(a). Initially, a sheet of the selected polyethylene (PE) material and an aluminum pipe were used, as shown in Fig. 6(b). The PE sheet was wrapped around the aluminum pipe. Instead of creating multiple layers, the sheet was overlapped by approximately 5 mm and then cut to achieve a single layer. Wrapping the sheet in multiple layers would make inversion more difficult due to increased thickness, thereby raising the pressure required for inversion and potentially causing air leakage. Finally, one of the overlapping edges was welded using a spatula-type sealer. The soft growing actuator produced with this method is depicted in Fig. 6(c). The aluminum pipe around which the PE sheet was wrapped had an outer diameter of 6 mm, matching the required inner diameter of the soft growing actuator. To ensure an extension length of up to 230 mm, the total length of the soft growing actuator was set to 280 mm.

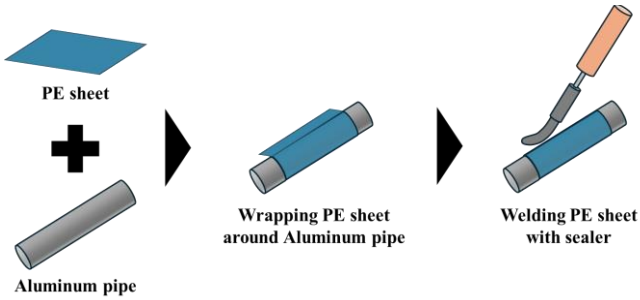

(a) Fabrication method of soft growing tube.

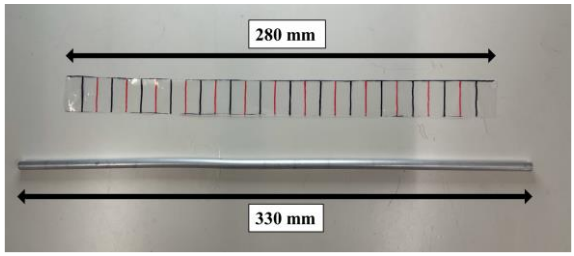

(b) PE sheet and Aluminum pipe.

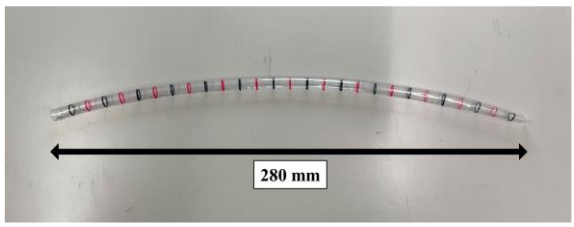

(c) Soft growing tube.

Figure 6. Development of soft growing tube.

IV. BASIC CHARACTERISTICS EXPERIMENT

This chapter describes the basic characteristic experiments of the developed soft growing actuator.

A. Purpose of the Simulation

To confirm the operation of the fabricated soft growing actuator, an air-pressure application experiment was conducted. The appropriate applied pressure was determined based on the relationship between elongation and time.

B. Simulation Conditions

The compressor was connected to an air regulator, and the air tube attached to the air regulator was directly connected to the fabricated soft growing actuator. The soft growing actuator had an inner diameter of 6 mm, an overall length of 280 mm, and an extendable length of 140 mm. The direct connection between the pneumatic tube and the soft growing actuator prevents the actuator from being folded back into the pneumatic tube, thereby limiting the possible extension length to 140 mm, which is half of the total length. This limitation arises from the absence of a pressurization chamber. Despite this, the 140 mm elongation was deemed sufficient for evaluation in the basic characteristic experiments.

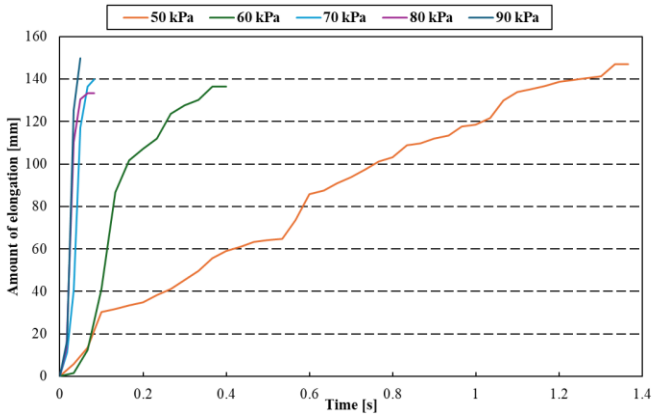

Figure 7. Elongation of soft growing actuator at each applied pressure.

The applied pressure was incrementally increased in 10 kPa steps from 10 to 100 kPa, and 10 extension experiments were conducted. Using video footage captured during the experiment, Kinovea software was employed to track the trajectory of the actuator. Graphical data were obtained showing the relationship between the tip extension of the soft growing actuator and the extension time.

C. *Results and Discussion*

Fig. 7 shows the relationship between time and the extension of the soft growing actuator for each applied pressure. At pressures of 10–30 kPa, no elongation was observed. At 100 kPa, the inverted elongated tube could not withstand the pressure, leading to a hole at the junction point of the tube. At 40 kPa, elongation reached its maximum after 18.0 s, which is significantly longer than the elongation times observed at other pressure levels; therefore, these results are excluded from the graph. Within the 70–90 kPa range, there was no significant difference in elongation time or extent, with specimens extending to their full length within 0.1 s. In this experiment, the soft growing actuator was evaluated without an attached cystoscope or spatial constraints such as those inside the urethra. Thus, the elongation under actual usage conditions might be more gradual compared to this experiment. It can be inferred that an air pressure range of 70–90 kPa allows for adequate elongation. Consequently, 80 kPa was selected as the applied pressure for the experiments conducted in the S-tube, as described in the next section.

V. Experiment in S-pipe

In this section, we describe an experiment in which a soft growing actuator was used to pull a wire imitating a cystoscope and extend it within an S-tube designed to mimic the urethra.

A. *Purpose of the Simulation*

We verified whether the soft growing actuator could pull a wire imitating a cystoscope through an S-tube, as shown in Fig. 8. In this experiment, a pressurization chamber was positioned between the soft growing actuator and the pneumatic tube to serve as a storage space for the inverted portion of the actuator and wire.

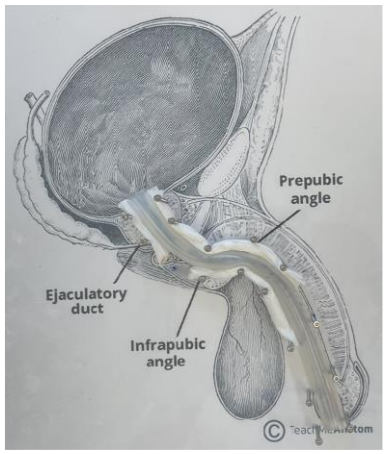

Figure 8. S-tube used in the experiment [5].

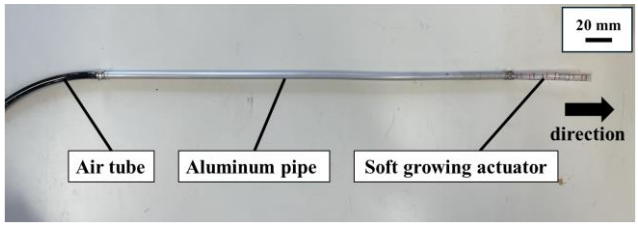

Figure 9. Appearance of experimental equipment.

B. *Simulation Conditions*

Fig. 9 shows the appearance of the soft growing actuator and the pressurization chamber used in the experiment. For this simplified setup, an aluminum pipe was used as the pressurization chamber. The procedure involved inverting the soft growing actuator and attaching a wire that mimicked a cystoscope to its tip. The wire and the inverted portion of the actuator were then placed inside the aluminum pipe, which was connected to the actuator. Finally, the air tube connected to the air regulator was attached to the aluminum pipe. The lengths of the various sections were as follows:

- Soft growing actuator
  Inner diameter 6 mm, total length 280 mm, extendable length 200 mm
- Wire
  Outer diameter 3 mm, length 100 mm
- Pressure chamber
  An aluminum pipe with an outer diameter of 6 mm and length of 330 mm was substituted.

The soft growing actuator was extended within an S-tube that mimicked the urethra by applying an air pressure of 80 kPa. The S-tube, made of rubber tubing, was designed to replicate the male urethra [5], as shown in Fig. 8. It had an inner diameter of 9 mm and a length of 180 mm, corresponding to the male urethra's diameter of 7–15 mm and length of 180–200 mm. Using video footage captured during the experiment, Kinovea software was employed to track the trajectory of the actuator. Graphical data were obtained showing the relationship between the elongation of the actuator tip and the elongation time.

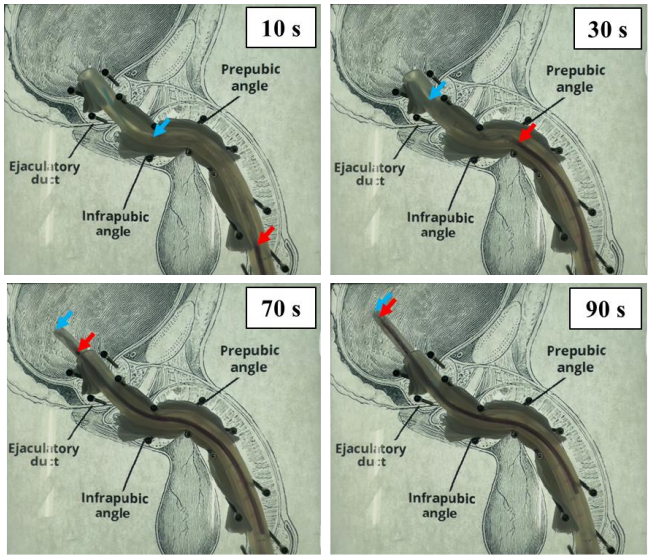

Figure 10. Extension of soft growing actuator in S-tube after 10, 30, 70, and 90 seconds. The blue arrow indicates the position of the tip of the soft growing actuator, and the red arrow indicates the position of the tip of the wire.

C. *Results and Discussion*

Fig. 10 shows the soft growing actuator with an air pressure of 80 kPa, pulling the wire into the S-tube. Fig. 11 presents a graph depicting the relationship between the elongation of the tip of the soft growing actuator and the elongation time. The actuator achieved its maximum extension, with the tip reaching its maximum possible extension length of 200 mm. The elongation exhibited three distinct intervals: (a) 1.5–19 s: This section shows the time when the tip of the soft growing actuator navigated through the second curve of the S-tube. The reduced elongation in this interval is attributed to the actuator being bent in the direction of the welded edge, as illustrated in Fig. 6(c). This bend required the actuator to turn away from the bend, which slowed down the extension process. (b) 20–47 s: During this period, the wire passed through the two curves of the S-tube. The reduced elongation observed in this interval is due to the wire causing a slight blockage inside the soft growing actuator. (c) 50–88 s: This section shows the time just before the actuator reaches its maximum elongation. The reduced elongation is due to the area near the tip of the actuator becoming stiffer due to the connection with the wire. This increased stiffness raises the force required for the reversal near the tip, resulting in reduced elongation as the actuator approaches its maximum length. In the future, we aim to address the causes of reduced elongation and achieve elongation within shorter timeframes. Additionally, the S-tube used in this experiment is a rubber tube with uniform thickness and material. Therefore, it does not fully replicate the internal shape of the urethra or the slipperiness of the urethral wall. Moving forward, we will develop a urethra model that replicates its shape and slipperiness, and work on advancing the design of the soft growing actuator that considers allowable pressure and other factors from the perspective of safety.

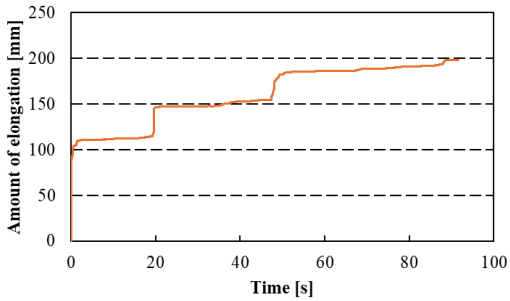

Figure 11. Elongation of the soft growing actuator in S-pipe.

VI. Conclusion

This paper proposes a compact, invertible soft growing actuator made of low-friction material for a painless automatic insertion mechanism. The optimal applied pressure was determined based on the elongation-time relationship of the actuator under air pressure. The actuator was successfully extended in an S-tube with a cystoscope-like wire, achieving a maximum length of 200 mm. Future plans include developing a pressurized chamber with an automatic mechanism for feeding and withdrawing the cystoscope. Additionally, we will verify the capability of the actuator to pull the cystoscope and observe its performance using the cystoscope's camera.

References

[1] National Cancer Institute, "What Is Bladder Cancer? - NCI," https://www.cancer.gov/types/bladder, (accessed Sep. 2024).

[2] F. Bray et al., "Global cancer statistics 2022: GLOBOCAN estimates of incidence and mortality worldwide for 36 cancers in 185 countries," CA Cancer J Clin, vol. 74, no. 3, 2024, pp. 229-263.

[3] Y. Xu et al., "Application of nanotechnology in the diagnosis and treatment of bladder cancer," Journal of nanobiotechnology, vol. 19, no. 1, 2021.

[4] Olympus America, "Flexible Cystoscopy," https://medical.olympusamerica.com/procedure/flexible-cystoscopy, (accessed Sep. 2024).

[5] TeachMeAnatomy, "The Urethra - Male - Female - Anatomical Course," https://teachmeanatomy.info/pelvis/viscera/urethra/, (accessed Sep. 2024).

[6] P. Valdastri et al., "A New Mechanism for Mesoscale Legged Locomotion in Compliant Tubular Environments," in IEEE Transactions on Robotics, vol. 25, no. 5, 2009, pp. 1047-1057.

[7] P. Glass, E. Cheung and M. Sitti, "A Legged Anchoring Mechanism for Capsule Endoscopes Using Micropatterned Adhesives," in IEEE Transactions on Biomedical Engineering, vol. 55, no. 12, 2008, pp. 2759-2767.

[8] H. Yamamoto et al., "Total enteroscopy with a nonsurgical steerable double-balloon method," Gastrointestinal Endoscopy, vol. 53, no. 2, 2001, pp. 216-220.

[9] T. Takamatsu et al, "Robotic endoscope with double-balloon and double-bend tube for colonoscopy," Scientific Reports, vol. 13, no. 1, 2023.

[10] E. W. Hawkes et al., "A soft robot that navigates its environment through growth," Sci. Robot. 2, eaan3028, 2017.

[11] X. Pi, I. A. Szczech and L. Cao, "A Retractable Soft Growing Robot with a Flexible Backbone," 2023 IEEE/RSJ Int. Conf. on Intelligent Robots and Systems (IROS), Detroit, MI, USA, 2023, pp. 2477-2484.

[12] Z. Wu et al., "Towards a Physics-Based Model for Steerable Eversion Growing Robots," in IEEE Robotics and Automation Letters, vol. 8, no. 2, 2023, pp. 1005-1012.

[13] A. Ataka and A. P. Sandiwan, "Growing Robot Navigation Based on Deep Reinforcement Learning," 2023 9th Int. Conf. on Control, Automation and Robotics (ICCAR), Beijing, China, 2023, pp. 115-120.